UCLA
COMPUTATIONAL AND APPLIED MATHEMATICS

Vapor-Liquid Interfacial Dynamics and Related Liquid Nitrogen Boiling on Perforated Plates

B. Miller
B. Merriman
K. Rafique
S. Osher
N. Noushkam
A. Spletzer
T.H.K. Frederking

August 1999

CAM Report 99-26

Department of Mathematics
University of California, Los Angeles
Los Angeles, CA. 90095-1555

http://www.math.ucla.edu/applied/cam/index.html

ELSEVIER

Cryogenics 39 (1999) 389–397

Cryogenics

Vapor–liquid interfacial dynamics and related liquid nitrogen boiling on perforated plates[1]

B. Miller, B. Merriman, K. Rafique, S. Osher *, N. Noushkam, A. Spletzer, T.H.K. Frederking*

5531 Boelter Hall, University of California, Los Angeles, CA 90095, USA

Abstract

For the switch from terrestrial gravity ("1*g*") to micro-gravity, we investigate vapor–liquid interfaces and their control in simulation studies and experiments. An improved level set method is presented for vapor bubble kinematics prediction. In view of a wide range of vapor bubble dynamics phenomena, our initial experimental investigations have focused on film boiling in and near perforated plates immersed in liquid nitrogen. A "zeroth order" approximation of transport based on minimum energy expenditure rates provides information on mean field vapor thickness. We have measured thermal conductance for the zero net mass flow case and finite mass flow. The data are compared with results obtained in comparison runs for single solid plates.

Keywords: Space cryogenics; Two-phase flow; Heat transfer; Heat exchangers

Nomenclature

a	base of triangular unit cell
A	area
B	bond number
c_p	specific heat at constant pressure
C_T	thermal conductance, h A
d	distance to vapor–liquid interface
d_h	hole diameter
D	viscous stress tensor
D_b	vapor bubble diameter
g	gravitational acceleration
h	heat transfer coefficient
H	enthalpy
k	thermal conductivity
n	vector normal to interface
P	pressure
Q	heat flow rate
R	radius of bubble
Re	Reynolds number
s	plate thickness
t	time
T	temperature
u	velocity (u,v)
x	spatial coordinate, x-direction
y	spatial coordinate, y-direction
α	surface tension
α_m	model constant
β_m	model constant
η	boundary condition parameter in y-direction
ϕ	level set function
κ	curvature
μ	shear viscosity
ρ	density
$\Delta\rho$	saturated fluid difference: liquid minus vapor value
τ	time constant
Ω	domain set
ξ	boundary condition parameter, x-direction
ψ	stream function

Subscripts

b	vapor bubble
conv	convection

* Corresponding authors. Tel.: + 1-310-825-4541 (exper.: T.H.K. Frederking). Tel.: + 1-310-825-1758 (CDF: S. Osher)

[1] Paper presented at the 1997 Space Cryogenics Workshop, Eugene, OR, USA, 4–5 August 1997.

0011-2275/99/$ - see front matter
PII: S0011-2275(99)00042-9

diff	diffusion
e	exterior fluid phase
exp	experimental value
g	gravity-related value at "1g"
o	time zero
tot	total value
spin	spinodal

1. Introduction

The present paper is subdivided into two parts: first simulation studies are addressed; second, experiments with perforated plates are reported selecting film boiling in liquid nitrogen as representative cryoliquid. It is noted that additional, parallel research efforts are ongoing at elevated temperatures at UCLA referred to in the subsequent discussion.

2. CFD simulation of single bubble dynamics

To understand the vapor–liquid dynamics and mechanisms of boiling in liquid nitrogen, the following scenario is considered: a single bubble formation is performed in a rectangular domain. Fig. 1 depicts the domain. The Navier–Stokes equations are solved over the rectangle as described below. A more detailed derivation has been given in Sussman [1].

The equations are applied to the problem of a bubble of one fluid moving in another fluid. The density and viscosity inside the bubble are denoted by ρ_b and μ_b, and exterior to the bubble as ρ_e and μ_e. The equations of motions are then:

$$u_t + (u\cdot\nabla)u = g + 1/\rho(-\nabla P + \nabla\cdot(2\mu D) + \alpha\kappa\delta(d)n) \quad (1)$$

$$\nabla\cdot u = 0 \quad (2)$$

where $u = u(u,v)$ is the fluid velocity, $\rho = \rho(x,t)$ is the fluid density, $\mu = \mu(x,t)$ is the fluid shear viscosity, D is the viscous stress tensor, g is the gravitational acceleration, and P is the fluid pressure. The final term in Eq. (1) is due to the surface tension and is derived in Chang et al. [2]; α is the surface tension coefficient, κ the local mean curvature of the interface; $\delta(d)$ is the Dirac delta function of d, the distance to the interface, and n is the outward unit vector normal to the bubble interface. Since the fluids are immiscible, the density and viscosity simply convect along with the fluid.

$$\rho_t + (u\cdot\nabla)\rho = 0 \quad (3)$$

$$\mu_t + (u\cdot\nabla)\mu = 0 \quad (4)$$

The problem formulation specifies Dirichlet conditions on u. For the bubble problem in a closed box choose

$$u = 0 \quad (5)$$

To non-dimensionalize the equations, it is necessary to choose a characteristic speed and length. For the bubble motion problem, a convenient choice for the characteristic length is the initial radius R of the bubble. After non-dimensionalization, the equations of motion (Eq. (1)) become

$$u_t + (u\cdot\nabla)u = g_u + 1/\rho(-\nabla P + 1/\mathrm{Re}.\nabla\cdot(2\mu D) + 1/B\kappa\delta(d)n) \quad (6)$$

Eq. (6) can be abbreviated as $u_t = L(u) - 1/\rho(-\nabla P)$, where the operator L defines the remaining terms in the equation. The dimensionless density and viscosity have the value 1 outside the bubble, and (ρ_b/ρ_e) and (μ_b/μ_e) inside the bubble. In the bubble problem, $\mathrm{Re} = (R^{1.5}\ (g)^{0.5}\ \rho_e/\mu_e)$ and $B = \rho_e\ g\ R^2/\alpha$ are the Reynolds and Bond numbers. The dimensionless gravity term is $g\ u = (0, -1)$.

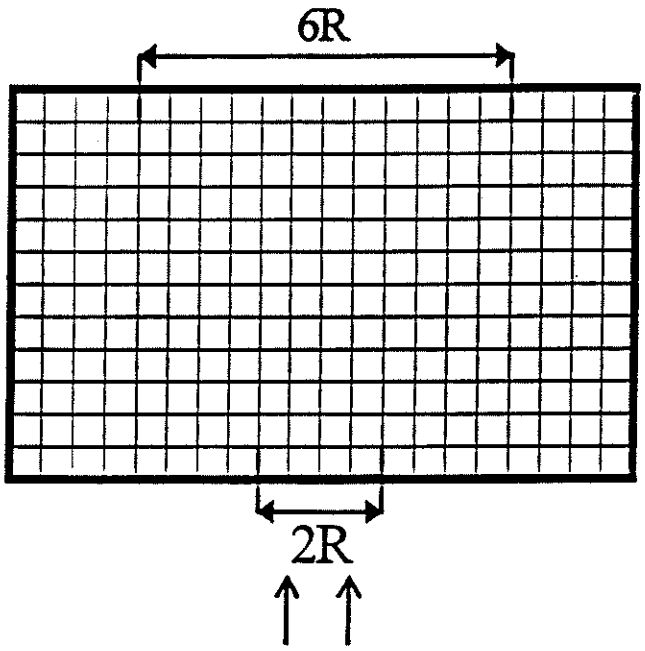

Fig. 1. Simulation grid geometry: vapor injection domain at the bottom extends over two radii ($3R$).

2.1. Level set method

An improved level set method is necessary for successful simulation of the problem. Numerical difficulties due to large fluid property changes across the vapor–liquid interface (of order [1000]) are overcome by the

level set function. A basic description of the level set function is given by Sussman [1]. Topology changes, such as bubble formation and pinch-off, are easily treated through the use of the level set function. The strong discontinuities in fluid properties are smoothed across a few grid points on either side of the interface and treated as continuous functions.

2.2. Cryogenic micro-gravity flows

The above method is applied to simulate liquid nitrogen boiling on a perforated plate. A first approximation of the problem is to model it as an injection of gaseous nitrogen into a box (Fig. 1) containing liquid nitrogen under very low gravity conditions. This problem models the process occurring when heat is transferred to liquid nitrogen near a boundary causing bubbles of gaseous nitrogen to form. First, the method of Sussman [1] is applied to the problem, which necessitates a few modifications. Second, a fluid velocity has to be defined at the injection site. This makes the determination of the dimensionless constants, the Reynolds and the Bond numbers, more straightforward. Thirdly, and more importantly, the no-slip boundary condition no longer applies.

Finally, the specification of the level set function is different. Initially, the box is entirely one fluid (liquid nitrogen), and the other phase (nitrogen vapor) is carried in through the inlet. This is accomplished by setting the level set function to be zero at the inlet, and negative in the ghost points outside the box, below the inlet. During the time evolution, the ghost points beneath the inlet are set explicitly to negative value.

In all the computer investigations, the method chosen was to specify an inlet port on the lower side of the box with a vertical velocity profile across the inlet. Because of incompressibility, it is necessary to specify an outlet port and outlet velocity so that

$$\int_{\partial\Omega} u.n = 0 \tag{7}$$

In all the tests, the inlet is on the bottom of the box and the outlet on top, so the integral condition becomes

$$-\int_{\text{inlet}} v\,\mathrm{d}x = \int_{\text{outlet}} v\,\mathrm{d}x \tag{8}$$

where v is the vertical component of velocity specified on the inlet or outlet.

In Sussman [1], the Navier–Stokes equations are expressed as $u = L(u)$, where $L(u)$ contains the convective, viscous, gravity and surface tension terms. The incompressibility condition is enforced by finding the divergence free part of L at each time step. This is done by solving

$$\nabla.(\rho\nabla\psi) = \nabla x\rho L \tag{9}$$

where ψ is the standard stream function. The free slip boundary conditions correspond to $\psi = 0$. Since $\mathrm{d}\psi/\mathrm{d}x = -v$ and $\mathrm{d}\psi/\mathrm{d}y = u$, we can now construct boundary conditions on ψ for the injection problem as follows.

For simplicity, let the box domain $\Omega = [0,1] \times [0,1]$. $\psi(0,0) = 0$, then

$$\begin{aligned}
\psi(x,0) &= -\int_0^x v(\xi,0)\mathrm{d}\xi \\
\psi(1,y) &= -\int_0^1 v(x,0)\mathrm{d}x + \int_0^y u(1,\eta)\mathrm{d}\eta \\
\psi(x,1) &= -\int_0^1 v(x,0)\mathrm{d}x + \int_0^1 u(1,y)\mathrm{d}y - \int_x^1 v(\xi,1)\mathrm{d}\xi \\
\psi(y,0) &= -\int_0^1 v(x,0)\mathrm{d}x + \int_0^1 u(1,y)\mathrm{d}y - \int_0^1 v(x,1)\mathrm{d}x \\
&\quad + \int_y^1 u(0,\eta)\mathrm{d}\eta
\end{aligned} \tag{10}$$

If Eq. (8) is satisfied, then this specification of boundary conditions on ψ will be consistent, that is $\lim_{y\to 0}\psi(y,0) = 0$. Numerous cases were run with these boundary conditions and include some plots of the injection process evolution.

In applying the new method to this injection problem, some difficulties were encountered in specifying correct boundary conditions [12–14].

The solution procedure can be summarized as follows:

1. Initialize level set function $\phi(x,0)$ to be the assigned distance to the initial interface. Set velocity u = 0.
2. Advance u and ϕ one time step using TVD Runge–Kutta scheme with the projection method.
3. Reinitialize ϕ.

2.3. Simulation results

Fig. 2 shows the time evolution of the injection process in the absence of surface tension. Note the effect of no surface tension: the trail of vapor that follows the bubble into the domain. In contrast, Fig. 3 shows how the presence of surface tension in the injection flow

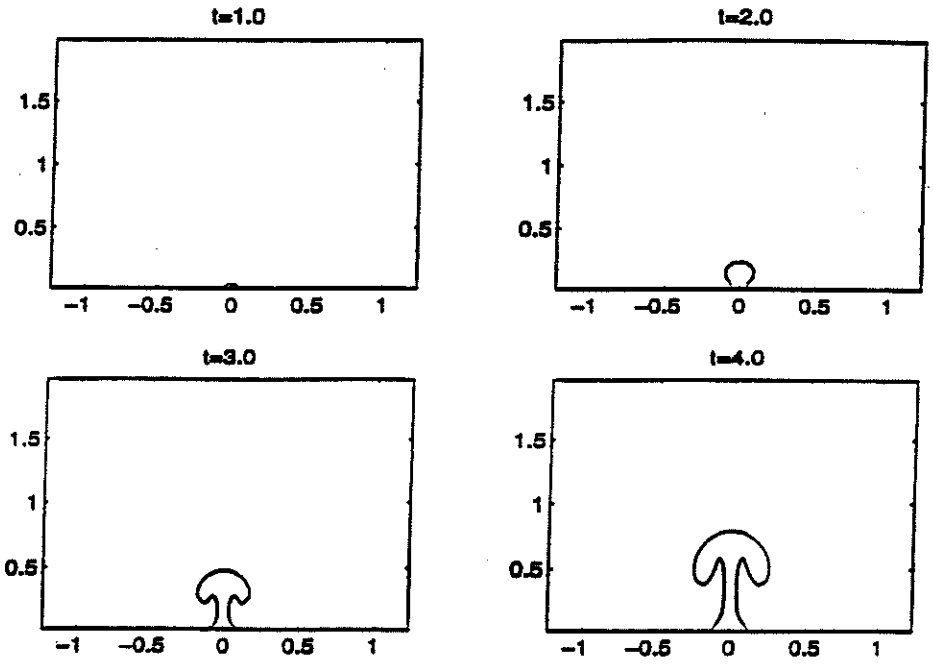

Fig. 2. Interfacial kinematics simulation: run with zero surface tension at terrestrial gravity $1g$.

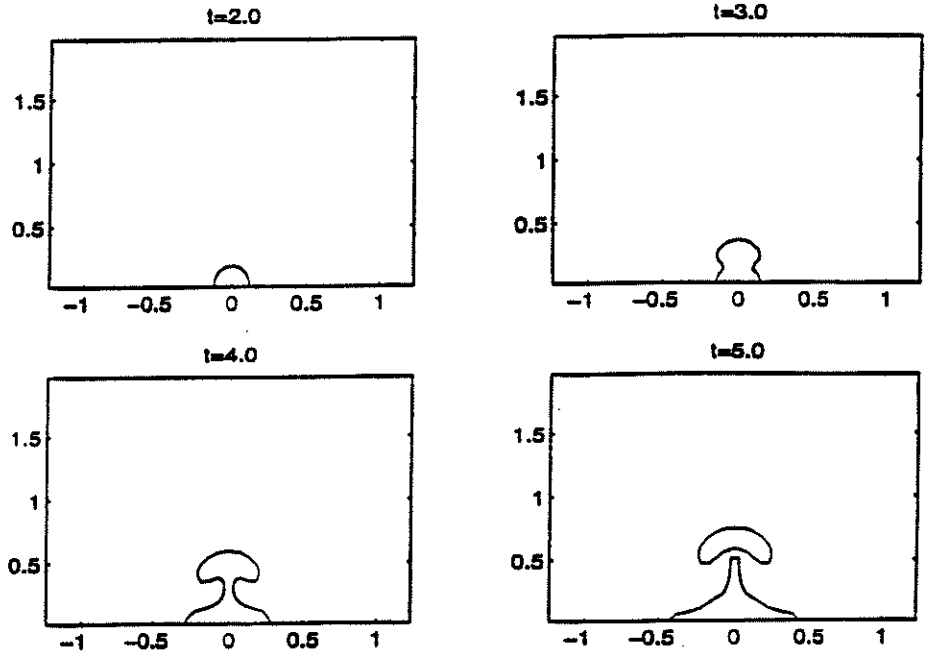

Fig. 3. Interfacial kinematics simulation: run with finite surface tension at terrestrial gravity $1g$.

causes the pinch-off of vapor. Fig. 4 shows the time evolution of the injection process for $1g$, and Fig. 5 presents $0.1g$ conditions.

The evolution of a single bubble in $0.1g$ (Fig. 5) shows a more lateral development. This is expected, because of a smaller buoyancy force. The pinch point for the bubble is delayed too. These results demonstrate the need for future studies both in numerical simulations and experimental verifications. The heat transfer coefficient will certainly be lowered in micro-gravity for the conditions investigated in the present simulation runs.

3. Experimental studies

The experiments have been conducted with perforated plates, i.e. miniaturized heat exchange components.

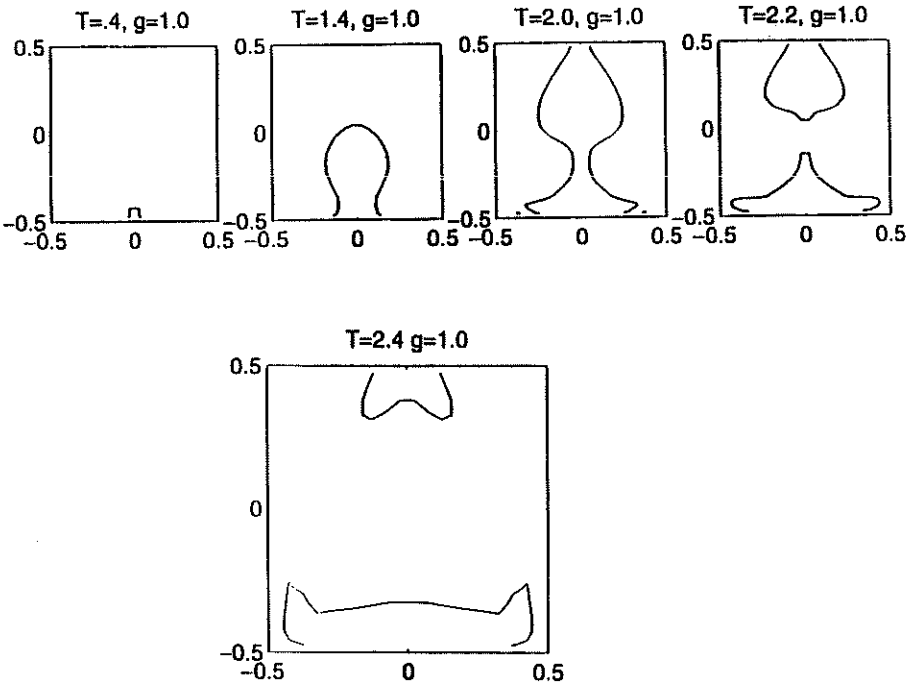

Fig. 4. Interfacial kinematics simulation: terrestrial gravity $1g$ and finite surface tension.

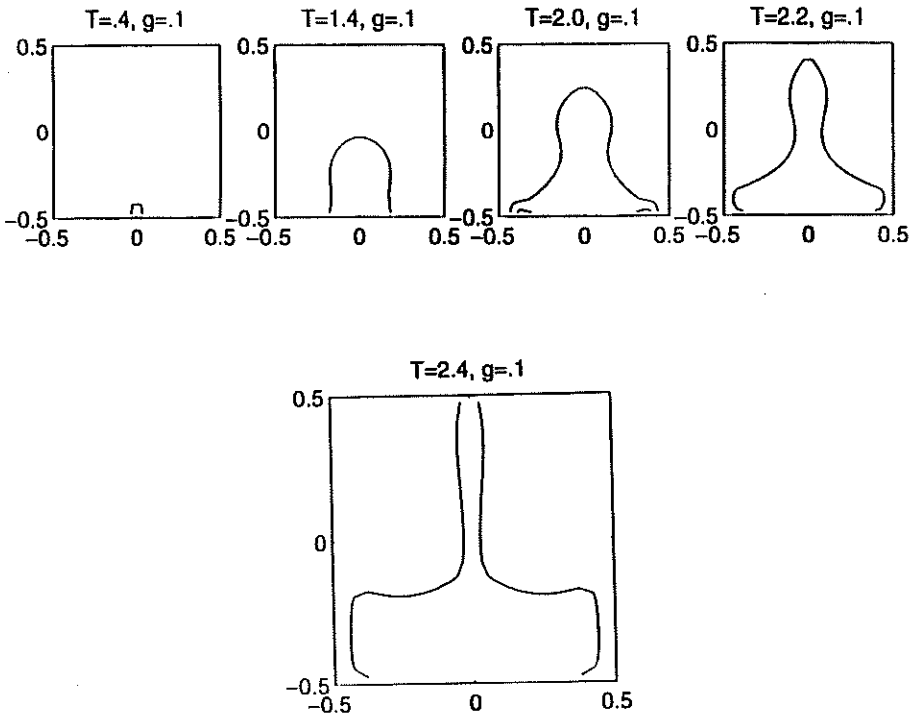

Fig. 5. Interfacial kinematics simulation: run at $0.1g$; finite surface tension.

They belong to an advanced category of subsystems potentially permitting small, efficient and low-cost systems, which do not jeopardize safety by "giant steps" in downsizing. Son and Dhir [7,8] report parallel studies on kinematics and experimental bubble growth at elevated temperatures. Further, there have been studies of perforated aluminum plates for the hydrogen sorption space cooler [9]; and of other Cu plates [10]. In addition, stainless steel exchangers with a width on the order of 100 μm have been reported [11].

The perforated plates used in our experiments have a duct diameter of $d = 0.356$ μm and a triangular "unit

cell" pattern (Fig. 6) (base a, perforated plate thickness s = 1.397 mm).

The objective at the beginning of the work was a critical comparison of simplified mean field theory prediction with data for vapor film thickness. The postulate of minimization of energy expenditure rates is used. It may be regarded as a special case of Ginzburg–Landau–Lifshitz system modeling [3]. This approach results in a simplified version of the laminar Nusselt–Bromley continuum theory for fluid convection (Incropera and DeWitt [4] list examples and related original literature references). The model vapor thickness provides guidance in comparison to the plate hole diameter.

In addition, heat transfer coefficients (h) in film boiling modes have been measured. They cover a rather wide range outside the reference value near 0.01 W/(cm^2 K) for a single sphere. The sphere reference case has been quoted often for pool boiling at $1g$.

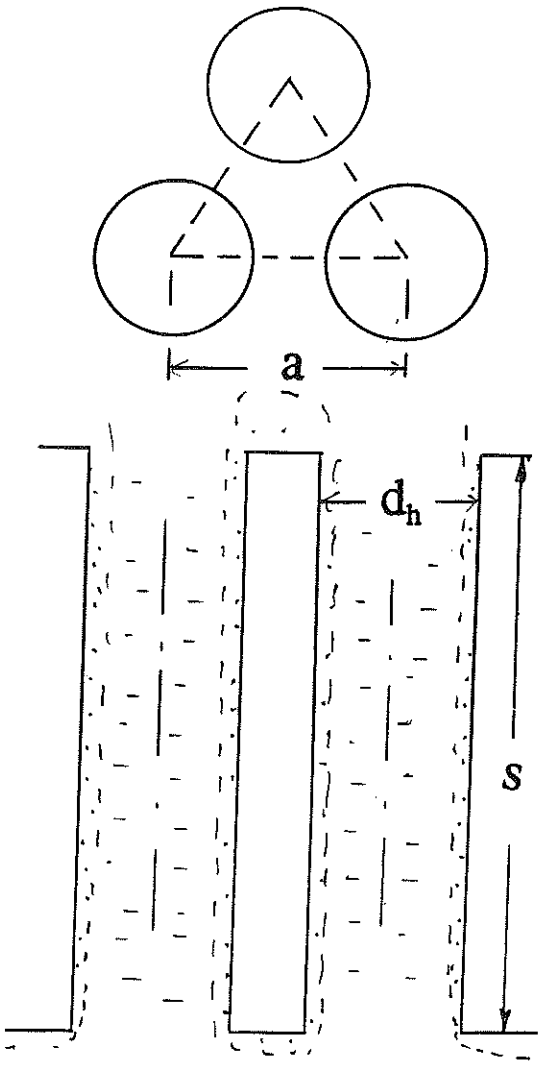

Fig. 6. Unit cell, schematically, not to scale; a base of triangular cell; a = 1.32 d_h (SEM record); duct diameter d_h = 0.356 mm, s height = plate thickness 1.397 mm; dashed line = fluid interface, schematically.

3.1. Experimental system modelling

3.1.1. Configuration

The classical film models of phase transitions may be considered "zeroth order" (mean field) approximations in the light of simulation work in the first part of this paper. We regard the unit cell of the hole-in-plate as base configuration (Fig. 6). The following domains are present: a vapor layer adjacent to the "hot" solid, a vapor–liquid interphase at saturation, and a liquid domain adjacent to the vapor film with the possibility of flow induced by the vapor's buoyancy in the "$1g$" gravity field.

3.1.2. Thermal transport scenario

We consider the following scenario: the solid temperature is above the spinodal temperature of the liquid. Thus, vapor blanketing is favored thermodynamically. Continuum conditions during the equilibration process cause a slow drop of the temperature (T) from the solid boundary to the vapor–liquid boundary at saturated fluid conditions. Pseudo-isothermal properties are substituted for the real property variations.

3.1.3. Property sets: fluid interfaces

There is a fluid interface domain of negligible thickness in the continuum treatment. Thus, we have separate vapor and liquid domains. In Fig. 6, the dashed line shows schematically the scenario of the modeling effort with a (dashed) vapor–liquid interface around a solid section of the unit cell of the perforated plate.

The saturated fluid interface is characterized by surface tension (α), saturated vapor density (ρ_v), and saturated liquid density (ρ_L). The related "$1g$" of terrestrial gravity leads to the effective pressure gradient $|\nabla P_g| = g\Delta\rho$. There is a characteristic vapor bubble size (Laplace length) in the gravity field (square root of surface tension divided by $|\nabla P_g|$). Because of saturation, the liquid domain is isothermal.

3.1.4. Property set: vapor domain

The vapor domain in the present approach has pseudo-isothermal properties such as thermal conductivity (k), shear viscosity (μ), density (ρ), and Prandtl number ($\mu c_p/k$), where c_p is specific heat at constant pressure. A pressure of 1 bar is assumed for numerical examples.

3.1.5. Transport model

We generate the vapor domain by sudden immersion of the plate in cryoliquid, i.e. liquid nitrogen. Since the solid (Cu) plate temperature is above the liquid spinodal, the immersion causes film growth toward a quasi-steady mean field thickness. The time needed for growth is on the order of magnitude of milliseconds. This initial time domain is omitted in our model. We generate quasi-steady transport by keeping the plate position fixed, letting

the system thermally equilibrate by slow, quasi-steady cooldown. Transport is assessed using the Y.I. Kim method of minimum entropy production rate, and minimum thermal energy expenditure for the present model system. There are two main entropy "generators": (1) the mean field conduction (diffusion) of heat flow (Q_{diff}) through the vapor film, and (2) the heat convected (Q_{conv}) via gravitational buoyancy acting on vapor. The sum of the contributions is the total heat flow rate Q_{tot}.

$$Q_{diff} + Q_{conv} = Q_{tot} \rightarrow \text{MINIMUM} \tag{11}$$

The order of magnitude (oom) of the diffusion term is

$$Q_{diff} = \text{oom } A_{diff} k \Delta T/\delta \tag{12}$$

("oom" is replaced by the tilde symbol "~" in the subsequent discussion). A_{diff} is the lateral fluid-wetted wall and the bottom area of the unit cell (Fig. 6). The top area has a large vapor domain with no significant contribution to Eq. (11). The area has an order of magnitude $A_{diff} = [(1/2)\pi d_h s + (1/3)d_h^2]$. The order of magnitude of the convection term is

$$Q_{conv} = \sim A_{conv} v(\rho \Delta H) \tag{13}$$

A_{conv} is the cross-sectional area available for vapor flow upward. A_{conv} has an order of magnitude of $(1/2)\pi d_h \delta$. The enthalpy difference per unit volume convected with the vapor flow is $\Delta H\rho$; ΔH is the "effective" latent heat equal to the phase change enthalpy difference augmented by the (average) sensible heat of vapor. In Eq. (13), v is the mean velocity of the vapor on the order of $(0.1)\delta^2|\nabla P_g|/\mu$. In our model we assess the mean vapor film thickness (δ) using the simplified version of postulate [11] from Kim [5]. There exists a minimum of Q_{tot} with respect to the vapor film thickness. The sum has the form $(\alpha_m/\delta + \beta_m\delta^3)$. Thus we obtain a particular thickness which minimizes the total Q-rate. The mean film thickness has order of magnitude $\delta^* = \sim[\alpha_m/(3\beta_m)]^{1/4}$, i.e.

$$\delta^* = \sim \{\mu k \Delta T s[1 + (1/3)(d_h/s)]/[(0.1)(3)|\nabla P_g|\rho\Delta H\}^{1/4} \tag{14}$$

(* dropped subsequently). At initial immersion of the plate in liquid nitrogen, we have a temperature difference of $\Delta T = 223$ K. The thickness (δ) has the value near 100 μm. Fig. 7 presents the normalized vapor thickness of the model for saturated liquid N_2 as a function of temperature difference down to the spinodal. The thickness is shown for half the present plate's thickness and for a plate of double thickness. As the hole diameter is reduced, the film thickness increases relative to d. Despite apparent order of magnitude agreement of our model with some features of fluid flow, there is a mismatch between the film thickness and the departing vapor bubble diameter $D_b = 2R$. In film boiling, we have D_b much larger than the Laplace length. This implies vapor collection from several unit cells for one departing bubble. The discrete vapor bubble set replaces the continuum film model, and it induces oscillations. Therefore, the present simulation studies are the starting point for a detailed assessment of the real interface kinematics.

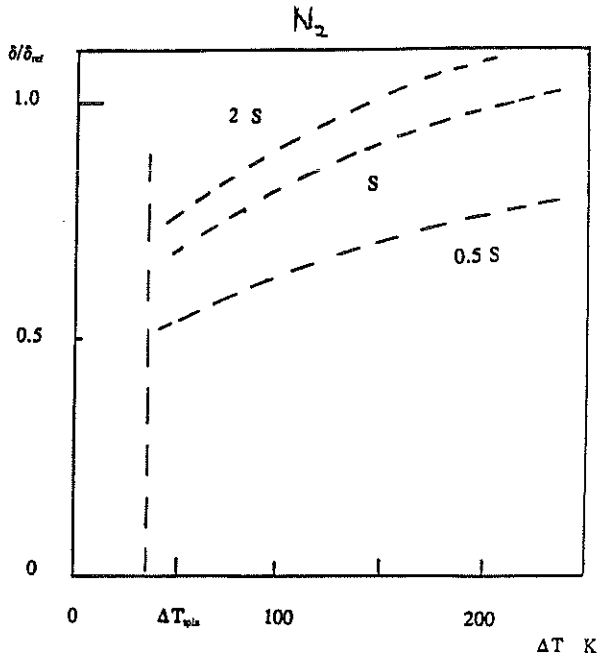

Fig. 7. Model vapor film thicknesses (normalized) versus temperature difference, $\Delta T_{spin} = T$ − difference at spinodal line of liquid decomposition.

3.2. Experimental runs

The runs have employed both the zero net mass flow (ZNMF) mode and the mode of finite mass flow (FMF). In order to realize both cases, a clamping (Cu) plate system has been used. It is a split plate system, leaving a central hole for the perforated plate. Fig. 8(a) presents a top view schematically. Fig. 8(b) is a schematic drawing of the cross-section. The clamping plate assembly is positioned horizontally to have open access for the FMF mode. The ZNMF mode is realized with a cover (G10) plate either above or below the perforated plate. In general, side wall heating requires some care. It is noted that contact conductances (Cu–Cu) vary considerably, including present runs after assembly, disassembly and reassembly. Additional comparison runs have been conducted with solid samples.

All samples have been oriented horizontally. The comparison runs have been conducted with a two-disk Cu assembly (2 inches = 2.54 cm diameter) and with a sample shown in Fig. 8(c). In one case, the "5-plus-1"

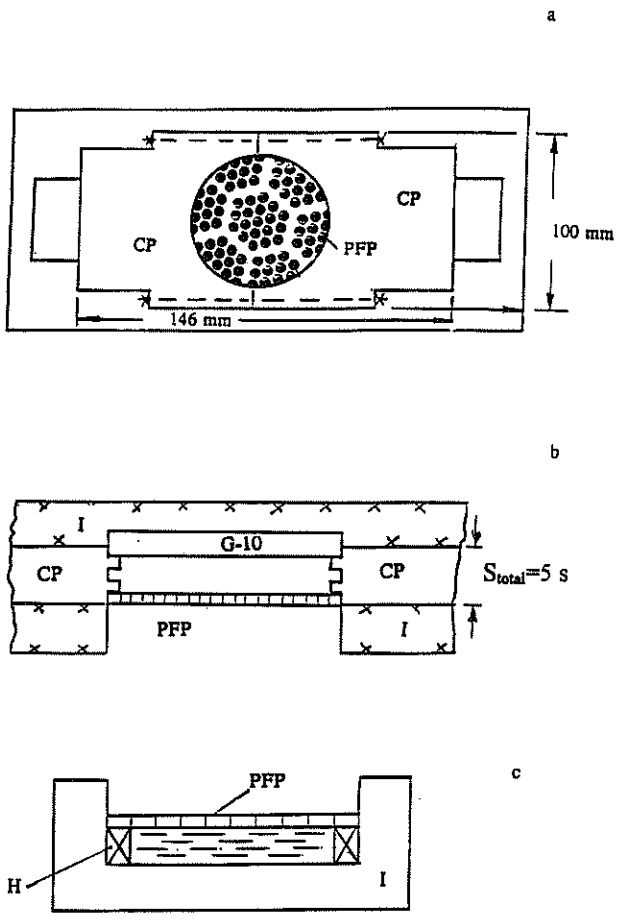

Fig. 8. Cu plate geometry, schematically. (a) Perforated plate (PFP) including Cu clamping plate (CP). (b) Schematic of the interface geometry: cross-section at PFP–CP interface with zero net mass flow, ZNMF (G10) barrier on top. (c) Geometry of "5-and-1" assembly with PFP; I, insulation; H, heater (Wadlow Electric Mfg. Company).

sample, the bare top and bottom surfaces have been exposed to fluid with heater windings mounted laterally. Subsequently, after insulation installation, the assembly has been augmented to the set-up "5-plus-1 plus perforated plate", with the perforated plate mounted on top. In this case, the ZNMF mode is imposed.

Fig. 8(b) includes a schematic drawing of the clamping plate's inner circle domain. This geometry includes three grooves fitting the perforated plate diameter. Initially, in the FMF runs, the plate has been mounted in the middle groove. In ZNMF runs, the plate has been inserted into the outer groove. Fig. 8(b) shows the ZNMF plate, the G10 insulating disk on top of the assembly and perforated plate mounted in the top position.

3.3. Results

3.3.1. Thermogram examples

Chilldown is initiated at time zero ($t = 0$). The temperature–time derivative $|(dT/dt)|_o$ at time $t = 0$ is given to first order by $\Delta T_o/\tau$; τ = time constant. Temperatures are measured with thermocouples (type "E", chromel–constantan). In the data reduction, the continuum model interpretation is based on heat supply in the form of the sample's excess enthalpy ΔH.

The resulting time constant is proportional to the mass per area (m/A) participating in the cooldown process;(h, thermal conductance):

$$\tau = c_p(m/A)/h \tag{15}$$

(where c_p is specific heat of copper at 300 K, 0.385 J/(cm^3 K)). Fig. 9 presents thermogram examples. There are subtle influences of lateral disk boundaries exhibited in Fig. 9 for the nearly "bare" comparison sample ("5-plus-1"). The insulation around the heater windings is asymmetric, causing a thermogram shift when the horizontal orientation is changed from zero to 180 degrees.

Time constants are shown in Fig. 10 versus the mass per area (m/A) wetted by fluid. The majority of data sets was collected with the perforated plate/clamping plate assembly (Fig. 8(a) and (b)). The time constants, observed in all the runs including solid samples, resulted in h-values in the range from above 0.01 W/(cm^2 K) down to 0.005 W/(cm^2 K). The corresponding vapor thickness (δ_{exp}) of the experiment is assessed using the order of magnitude of the film model described above:

$$\delta_{exp} = \sim (k/h) \tag{16}$$

From the data we obtain the experimental values of the thickness from δ_{exp} on the order of magnitude 300 μm, in agreement with the mean field vapor thickness of our zeroth order model. For further experimental details we refer to Spletzer et al. [6].

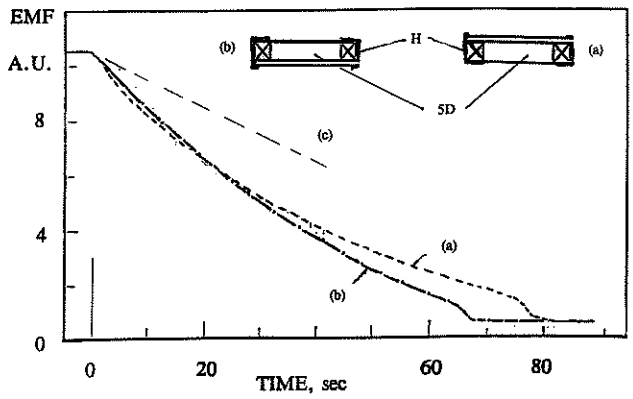

Fig. 9. Thermogram examples (EMF versus time): multi-disk horizontal systems; (a) "5-plus-1" sample; "large area up"; 6.14 cm diameter matching PFP diameter); 5D = 5-disk (2 inches diameter) assembly; H = heater; (b) "5-plus-1" sample "large area down"; (c) "5-plus-2" horizontal sample, "large area up"; 6.14 cm Cu plate and PFP on top; zero net mass flow (ZNMF) mode.

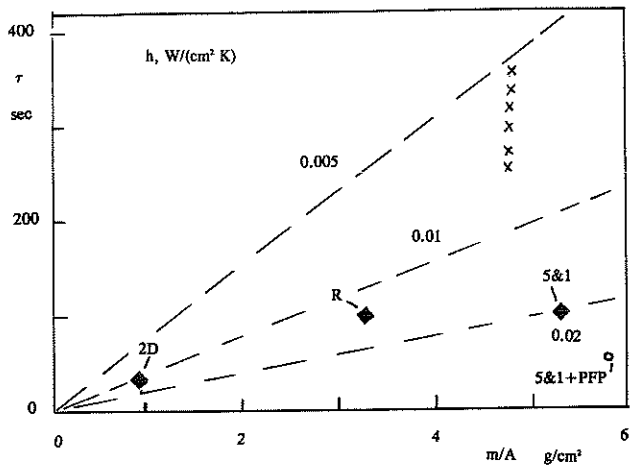

Fig. 10. Time constants versus mass (m) per area (m/A); a fluid-wetted area. Straight lines depict constant heat transfer coefficient (h); R, sphere reference; 2D, horizontal disk (courtesy Jimmy Leung); 5-and-1 + perforated plate (Parsha Ghodsi and Gary Ma); 5-and-1 (F. Ewald); × , zero net mass flow (ZNMF) and finite mass flow (FMF) runs with the horizontal perforated plate (Fig. 8(a)).

4. Concluding remarks

Simulation results demonstrate the usefulness of the level set method. The vapor bubble domain evolution in space and time displays detailed features of physical bubbles in the range of parameters selected.

Perforated plate runs at incipient cooldown with vapor film-impeded transport show considerable variations of heat transfer coefficients (h). Minor details of mode and surface conditions influence the data. Despite these variations, the order of magnitude of h known from vapor films on single solids is retained. Vapor film thickness agrees in order of magnitude with our zeroth order film model. In contrast, the absolute thermal conductance $C_T = hA$ is changed dramatically: there is an order of magnitude reduction in cooldown time as the solid horizontal plate is replaced by the perforated plate.

The vapor liquid interface simulations illustrate the artificial "film" nature of continuous domain models. The simulations are encouraging in their progress toward establishing a detailed interface kinematics at 1g and at micro-gravity. An account of bubble history is essential for extending knowledge beyond the classical "film picture".

Acknowledgements

We wish to thank our collaborators, NASA and research students for their input. In the experimental area the following persons are acknowledged with appreciation: Dr. John Hendricks, ACE; Lloyd French (JPL)-Micro-gravity flight trajectories; Peter Bischoff: data collection and reduction; Andrew Khang Le: model calculations; F. Ewald: 5-and-1 sample; Parsha Ghodsi and Gary Ma: 5-and-2 sample (104A, SQ97).

References

[1] Sussman M. A level set approach for computing solutions to incompressible two-phase flows. Ph.D. thesis, University of California, Los Angeles, 1994.
[2] Chang YC, Hou TY, Merriman B, Osher S. A level set formation of Eulerian interface computing methods for incompressible fluid flows. CAM Report 94-4, University of California, Los Angeles, 1994.
[3] Landau LD, Lifshitz EN. Statistical physics. London: Pergamon, 1958.
[4] Incropera FP, DeWitt DP. Fundamentals of heat transfer. New York: Wiley, 1981.
[5] Kim YI. Ph.D. thesis, University of California, Los Angeles, 1982.
[6] Spletzer A et al. In: Proceedings of the 3rd International Thermal Energy Congress (3rd ITEC), Kitakyusha, 1997:287–92.
[7] Son G, Dhir VK. Numerical simulation of a horizontal substrate placed beneath a heavier liquid. J Heat Transf (submitted for publication).
[8] Son G, Dhir VK. Numerical simulation of film boiling near critical pressures with a level set method. J Heat Transf 1998;120:183–92.
[9] Rodriguez JI, Mills AF. Heat transfer and flow friction characteristics of perforated-plate heat exchangers. Exp Heat Transf 1996;9:335–56.
[10] Viargues F, Claudet G, Seyfert P. Construction of perforated-plate heat exchanger for use in He II refrigerators. ICEC15 Proc 1994;325-8.
[11] Hofmann A. Parallel flow regenerator for pulse tube cooler application. Adv Cryog Eng 1998;43B:1627–33.
[12] Oha S, Sethian JA. Fronts propagating with curvature dependent speed, algorithms based on a Hamilton–Jacobi formulation. J Comput Phys 1988;79:12–49.
[13] Osher S. Lectures on Numerical Methods of Appl Math and CFD, UCLA, Math Dept.
[14] Rafique K, Miller B. Unpublished results.